Chapter 9
Optimization of the Experimental Set-up for a Turbulent Separated Shear Flow Control by Plasma Actuator Using Genetic Algorithms

Nicolas Benard, Jordi Pons-Prats, Jacques Périaux, Jean-Paul Bonnet and Gabriel Bugeda

Abstract Since 1947, when Schubauer and Skramstad (J Res: 69–78, 1947 [1]) established the basis of the technology with its revolutionary work about steady state tools and mechanisms for the flow management, the progress of the flow control technology and the development of devices have progressed constantly. Anyway, the applicability of such devices is limited, and only few of them have arrived to the assembly workshop. The problem is that the range of actuation is still limited. Despite their operability limitations, flow control devices are of great interest for the aeronautical industry. The number of projects investigating this technology demonstrates the relevance of in the Fluid Dynamic field. The scientific interest focus not only on the industrial applications and the improvement of the technology, but also on the deep understanding of the physical phenomena associated to the flow separation, turbulence formation associated to the final drag reduction aim. A clear example of what has been mentioned is the EC MARS research project (MARS project, FP7 project number 266326, [2]). Its objectives are aimed to a better understanding of the Reynolds Stress and turbulent flow related to both drag reduction and flow control. The research was carried out through the analysis of several flow control devices and the optimization of the parameters for some of them was an important element of the research. When solving a traditional fluid dynamics optimisation problem numerical flow analysis are used instead of experimental ones due to their lower cost and shorter needed time for evaluation of candidate solutions. Nevertheless, in the particular case of the selected flow control plasma devices the experimental measurement of the performance of each candidate configuration has been much quicker than a numerical

N. Benard (✉) · J.-P. Bonnet
Institut PPRIME - UPR 3346 – CNRS - Université de Poitiers - ISAE/ENSMA - SP2MI
Téléport2, Bd Marie & Pierre Curie, BP 30179, 86962 Futuroscope Chasseneuil Cedex, France
e-mail: nicolas.benard@univ-poitiers.fr

J. Pons-Prats · J. Périaux · G. Bugeda
International Center for Numerical Methods in Engineering (CIMNE),
c/Esteve Terrades 5, 08860 Castelldefels, Spain

J. Périaux · G. Bugeda
Universitat Politècnica de Catalunya (UPC), c/Gran Capità S/N, 08034 Barcelona, Spain

N. Qin et al. (eds.), *Advances in Effective Flow Separation Control for Aircraft Drag Reduction*, Computational Methods in Applied Sciences 52,
https://doi.org/10.1007/978-3-030-29688-9_9

analysis. For this reason, the corresponding optimisation problem has been solved by coupling an evolutionary optimization algorithm with an experimental device. This paper discusses the design quality and efficiency gained by this innovative coupling.

Keywords Turbulent separated shear flow control · Surface plasma actuator · Experimental optimization · Genetic algorithm

9.1 Introduction

Despite their limitations, flow control devices remain of great interest to the aeronautical industry. The number of projects investigating this advanced technology confirms the relevance of the technology. The scientific outcomes are not focussed only on industrial applications and the continuous improvement of the technology, but also on a better understanding of the physical phenomena associated to the flow separation including the turbulence formation linked to the ultimate reduction of drag.

An example of the above approach can be found in the EC MARS project [2]. The objectives of MARS aimed to provide a better understanding of the Reynolds Stress and the turbulent flow related to drag reduction and flow control. The research was carried out through the analysis and comparison of several selected flow control devices.

On the framework of the research activities of European and Chinese partners involved in the MARS project, the optimization of the parameters of some selected devices was an important task.

When solving a fluid dynamics optimisation problem in aerodynamics full numerical analysis software are used in many cases instead of experimental analysis software due to their lower cost and shorter time execution to feed the optimizer. Nevertheless, in the particular case of a selected flow control plasma device the experimental measurement of the evaluation of different configurations has been much faster than with a numerical flow analysis code. This is because numerical simulation needs to be at least of the level of hybrid RANS-LES to resolve the unsteady turbulent scales. For this reason, it has been decided to solve the corresponding optimisation problem by coupling an evolutionary optimization algorithm to an experimental plasma device.

This paper evaluate from the results the design quality and efficiency of this coupling on a Backward Facing Step.

This paper describes in six (6) sections the experimental and, optimization setups through an efficient software and hardware interface and the analysis of optimized results obtained on a Backward Facing Step (BFS) test case. Sections 9.2 and 9.3 describe the experimental and optimization setup respectively. Numerical results obtained with the experimental optimization setup are discussed in Sect. 9.4 while Sect. 9.5 presents conclusions and future of the innovative research.

9.2 Experimental Setup

The selected test case is the optimization of a Backward Facing Step (BFS) with the Plasma device. Design variables and objective functions for the optimization are described in the following sections.

9.2.1 Description of the Wind Tunnel

The model is installed in a closed-loop wind-tunnel on Fig. 9.1 having a moderate turbulent intensity (1%). The dimension of the test section is $300 \times 300 \times 1000\,mm^3$. All measurements are performed for a free-stream velocity of 15.6 m/s.

9.2.2 Description of the Step Model

The model includes a step having a height, h, of 30 mm and a span wise length of 300 mm. The model covers the full span wise and the expansion ratio equals to 1.1. This expansion ratio is high enough for reducing the influence of stream wise pressure gradient along the wall of the wind-tunnel on the mean flow reattachment position. The aspect ratio (channel width on step height) is larger than 10 as recommended by the literature to assure a two-dimensional flow in the centre of the wind tunnel. Measures are conducted for a fixed Reynolds number of 30,000 based on h, the height of the step.

9.2.3 Description of the Plasma Device

The step model is made of several pieces; in particular it has been designed in order to have a removable part (see Fig. 9.2). The removable part corresponds to the step geometry and is made of a 3-mm thick machined PMMA piece. So, the model can be

Fig. 9.1 Closed-loop wind tunnel dedicated to backward facing step measurements

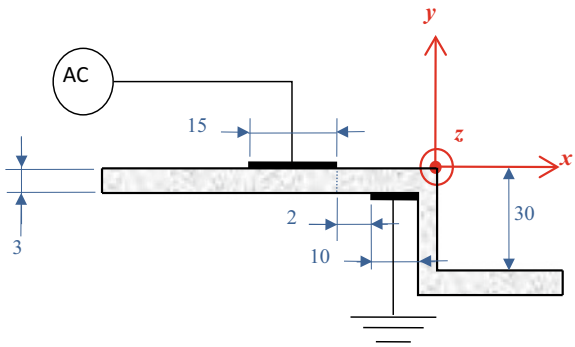

Fig. 9.2 Sketch of the DBD plasma actuator with details on electrode arrangement

used as dielectric barrier directly. This common electrode arrangement is introduced in Fig. 9.2. As shown, the active and the grounded electrode have a length of 15 and 10 mm respectively and the gap between them is fixed at 2 mm. By construction, the electrode protuberance into the flow is limited to the electrode thickness (i.e. 60 μm) and then the initial turbulent boundary layer characteristics are not modified by the actuator.

In all experiments, a TREK® (model 30/20A) high voltage power amplifier equipment is used as voltage source for the DBD. This amplifier generates a maximum output voltage of $\pm$30 kV (tension gain 3000 V/V) and a maximum output current for AC peak of $\pm$40 mA at 600 W maximum power (slew rate 500 V/μs).

9.2.4 Description of the LabVIEW Software and Transducer Setup Interfaces to Operate the Wind Tunnel

In the present investigation, an optimization study based on experimental results from the wind-tunnel is conducted. The bottom wall downstream of the step has been equipped with pressure taps (55 pressure tabs from x/h = 1 to x/h = 9 with a spatial resolution of 0.15 h) (Fig. 9.3). A set of 32 unsteady pressure sensors (12 bits) with bandwidth of 2 kHz for max pressure of 250 Pa has been designed and packed in a dedicated rack. Output voltage signals of the pressure sensors are recorded by PXI hardware (2.16 GHz dual core) with 32 channels acquisition card (PXI-6259). This system includes a signal generator card (PXI-5402) for supplying the actuator by the electrical parameters defined by the optimizer while the output responses of the 32 sensors are recorded. The LabVIEW code manages the acquisition of the pressure sensors, estimation of the objective functions, the electric command of the actuator and it makes the interface between the wind-tunnel and the optimizer. The interface between the optimizer (.exe file) and the wind-tunnel is done via DOS command under LabVIEW and the input/output interactions are managed through ASCII files.

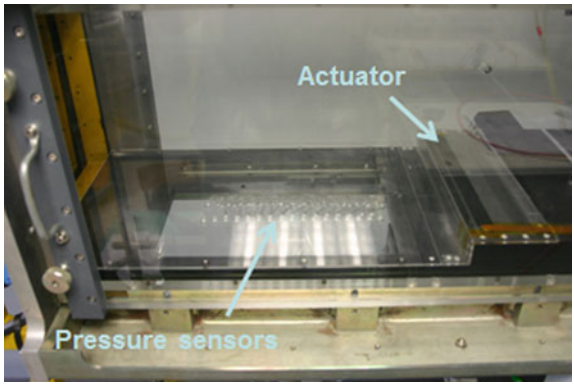

Fig. 9.3 Photograph of the step model equipped with a linear surface DBD actuator and 55 pressure taps

9.2.5 Description of the Design Variables/Input Parameters Selected

The control mechanism of plasma discharges is based on an electromechanical conversion meaning that all characteristics of the applied electrical signal have influence on the produced flow. As shown in literature [3], the voltage amplitude and driven frequency f_{ac} are responsible for the amplitude of the produced local flow, usually called electric wind. Higher are the applied voltage amplitude and frequency, higher is the induced maximum flow velocity. However, in all the cases the produced flow resembles a wall jet, tangent to the dielectric barrier. To maximize the induced flow velocity, frequency of kHz order is usually used. In order to amplify the interactions between the induced plasma flow and the natural flow having inner frequency content, the actuator is often operated in a modulated manner. Here, burst modulation is used meaning that the actuator is alternatively switched on and off at a frequency f_{bm} with a duty-cycle DC. Some illustrative results of the induced velocity profiles are introduced in Fig. 9.4 for 'steady' (Fig. 9.4a) and 'unsteady' forcing (unsteady forcing refers to burst modulation of the ac high-voltage signal, see Fig. 9.4b). Due to the fast response of any electromechanical converter in absence of any mechanical part, the driven frequency f_{ac} and the burst frequency f_{bm} induced periodic fluctuations in the produced flow, these fluctuations being at the supplied electrical frequencies.

In the framework of control optimization performed here, the design variables concern the voltage amplitude, the burst frequency and the duty-cycle considering that the driven frequency is fixed at $f_{ac} = 2$ kHz. In these conditions, it is well known that the mean amplitude of the produced flow increase with the voltage amplitude. The motivation for changing the burst frequency is that the flow is very sensitive to periodic excitations at the right frequency (i.e., excitation frequency matching with the preferred mode of the considered flow). The last design variable is the duty-cycle. High duty-cycle value means that the produced flow approaches steady flow conditions (i.e., small fluctuation amplitude) while low duty-cycle will emphasize the amplitude of the fluctuations but in this case the mean produced flow velocity is small.

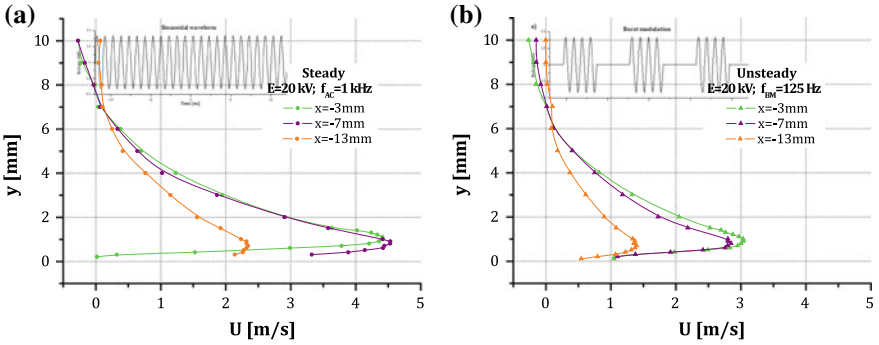

Fig. 9.4 Three stream wise velocity profiles induced by reference steady (**a**) and unsteady (**b**) actuation

Then, for flow control perspectives, a balance has to be found for producing a 'high' mean flow having 'high' fluctuation amplitude. All of these three parameters have strong influence on the performance of the control, this motivating for optimization studies using advanced algorithms.

9.2.6 Objective Functions Selected for Optimization

Two objective functions have been selected for the optimization. The first one concerns a mean quantity useful to demonstrate the potential of surface plasma to reduce reattachment downstream of the backward-facing step model. The location of the mean reattachment point is estimated by the position of the pressure fluctuation peak along the stream wise direction on the wall as recommended in literature [4] and illustrated in Fig. 9.5. The procedure simply consists of recording the 32 pressure signals on the bottom wall and computing each local pressure fluctuation amplitudes. Then a dedicated gradient-based algorithm seeks for the location of the maximal fluctuation, this point being related to the mean reattachment. Preliminary tests have shown that a correct estimation of the mean reattachment point requires 5–10 s to attain a converged value due to the unsteady character if the reattachment point. For this quantity, the estimated error is mainly caused by the spatial distribution of the sensors. Here, the reattachment is estimated within ± 0.15 h.

In order to extend the optimization to dynamic component of the flow a second objective function is considered. The spatial integral of the pressure fluctuations P' are performed all along the bottom wall (i.e., spatial integration of plot such as presented in Fig. 9.5). The pressure trace is assumed to be caused by the flow variations in the free shear layer developed from the step corner. Then, higher value of P', and thus higher value of the P' spatial integral, is supposed to be related to a more intense vortical flow activity. This is confirmed in Fig. 9.6 where the time-history of the pressure signals at different spatial position is plotted for the natural

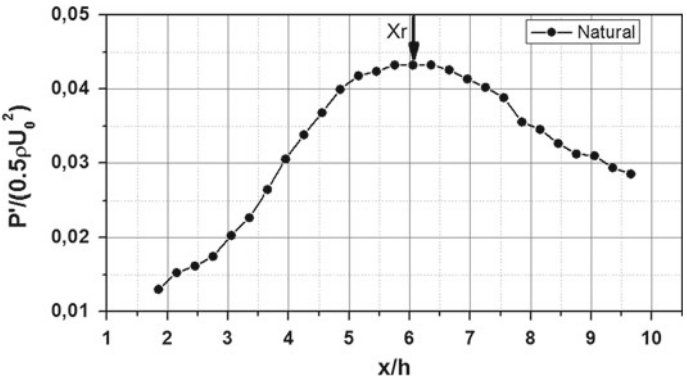

Fig. 9.5 Typical distribution of pressure fluctuations along the bottom wall downstream the step model

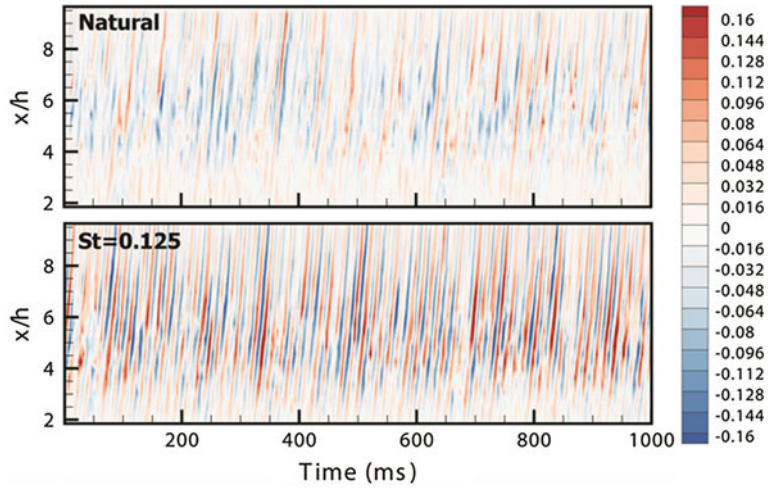

Fig. 9.6 Time-history of the wall pressure signature (normalized values) along the streamwise direction for natural and unsteady forcing by burst modulation at $f_{BM} = 65$ Hz ($St_h = 0.125$)

flow and flow controlled by a plasma discharge operated in burst modulation at 65 Hz. In both cases, the trace of the periodic fluctuations, i.e. the signature of the vortical flow structures, confirms that periodic flow is observed few step heights downstream the step corner. When forced at $St_h = 0.125$, large changes can be observed. The signature of the vortical flow structures is visible at a nearest position from the step corner (x/h ~ 3). The organization of these structures seems highly modified with a high coherence with downstream positions and a regularization in the periodicity of the vortex street. The spatial integral of the pressure fluctuation is largely increased in the case of actuation. Higher is the spatial integral, higher is the influence of the actuator on the vortical flow activity. The convergence rate of this integrated quantity

is lower than the mean reattachment as only 5 s are needed to achieve a converged value while the estimation error is limited to 3%.

9.3 The Moga Evolutionary Optimizer

More and more often, engineering design problems require a simultaneous optimization of several objectives associated to a number of constraints. Unlike single objective optimization problems, the solution can be a set of non-dominated solution well known as the Pareto optimal Front Solutions are compared to other solutions using the concept of Pareto dominance. A multi-criteria optimization problem can be formulated as follows:

Maximise/Minimise

$$f_i(x), i = 1, \ldots, N_f, \tag{9.1}$$

Subject to constraints:

$$g_j(x) = 0 \text{ and } h_k(x) \geq 0, j = 1, \ldots, N_g, k = 1, \ldots, N_h, \tag{9.2}$$

where f_i g_j h_k are, respectively, the objective functions with a total number of N_f, the equality constraints with a total number of Ng and the inequality constraints with a total number of N_h. x is an N_x dimensional vector where its arguments are the decision variables.

For a minimisation problem using a Pareto game, a vector x_1 is said partially less than vector x_2 if:

$$\forall i \; f_i(x_1) \leq f_i(x_2) \text{ and } \exists j \; f_j(x_1) < f_j(x_2), \tag{9.3}$$

In this case the solution x_1 dominates the solution x_2.

In Evolutionary Computation, optimisation algorithms evaluate and classify the value of objective functions between several different candidates in order to detect best to worst performance. The selection of the designs to be evaluated is depending on the selected optimisation algorithm. In the case of Genetic Algorithms (GAs), they define and evaluate multiple populations of design points in order to capture a number of solutions belonging to the Pareto set. Pareto selection ranks the population and selects non-dominated individuals for building the Pareto Front. A Genetic Algorithm that has capabilities for multi-objective optimisation is termed Multi-Objective Genetic Algorithms (MOGAs). Theory and applications of MOGAs can be found in Ref. [5–7].

The single-objective case is formulated in the same way, but limiting the number of objective functions (N_f) to be equal to 1. The problem can include equality and inequality constraints, as defined in the multi-objective problem, and the concept

of dominance is no longer used due to the fact that only one objective function is considered.

The selected optimizer used in this work is the Multi-Objective Genetic Algorithm (MOGA) module in Robust Multi-objective Optimization Platform (RMOP) developed at CIMNE. Details of RMOP can be found in Ref. [5–7]. The optimization platform enables the analysis of multi-objective problems using the hybridized techniques that combine Pareto-game and Nash-games.

Developing efficient optimization techniques is the most challenging task in the field of Evolutionary Algorithms (EAs) research due to the complexity of modern design problems. One of emerging techniques to improve an optimisation performance is the use of the Nash-equilibrium concept which will be acting as a preconditioner of global optimizer.

Lee et al. [8] introduced the concept of Hybridized Games (a Pareto and Nash coalition) coupled to a well-known MOEA. Non-dominating Sort Genetic Algorithm II (NSGA-II) [9] are used to solve Unmanned Aerial System (UAS) multi-objective Mission Path Planning System (MPPS) design problems and speed up with the Hybridized Games by 80% when compared to the original NSGA-II. In addition, Lee et al. [10] have also hybridized NSGA-II optimizer with Nash-Game strategies to study the dynamic speed up of Nash-Players via Hybridized Games in the capture of different shapes of Pareto fronts (convex, concave, discontinuous, …) with multi-objective mathematical functions A Hierarchical Asynchronous Parallel Multi-Objective Evolutionary Algorithm (HAPMOEA) [11] can be also hybridized to solve a real-world robust multidisciplinary design problem. Numerical results show that the Hybridized Games can improve up to 70% of the HAPMOEA performance while producing better Pareto optimal solutions. References [8] clearly describe merits of using Hybridized Games coupled to MOEA for engineering design applications which consider complex geometries with large number of design variables. The Hybridized Game concept has two major properties: the first is a decomposition of a multi-objective design problem split into several simpler ones handled by Nash-Players with their own design search space. The second one allowing Nash-Players to synchronise their elitist strategy with Global or Pareto Players and accelerate the optimization procedure by maintaining diversity by a dynamic strategy of the Nash-Players.

The optimizer used during the experimental optimization is a sub-version of the advanced genetic algorithm code [7, 11]. The simplified version of the optimization code is not using the parallel computing capabilities in order to avoid overloading the wind tunnel actuator with more than one individual at the same time.

9.4 The Plasma Wind Tunnel Optimization: Results

9.4.1 Inverse Reconstruction Problems with Plasma Wind Tunnel Analysis

The procedure of coupling an experimental Plasma active device with a numerical optimization code, as an analogic solver, has been carefully validated in order to ensure that the methodology is able to solve complex optimization problems. It has been decided to test the coupled experimental-numerical optimization procedure with the following three inverse problems:

(1) Problem 1: A single objective problem to recover a prescribed reattachment length
(2) Problem 2: A single objective problem to recover a prescribed P' integral value
(3) Problem 3: A multi-objective problem to recover both prescribed reattachment length and P' value.

All the three reconstruction problems (1), (2) and (3) use the same definition: Minimize

$$f_i(\boldsymbol{x_1}, \boldsymbol{x_2}, \boldsymbol{x_3}) = f_{pi}(\boldsymbol{x_1}, \boldsymbol{x_2}, \boldsymbol{x_3}) - f_{ei}(\boldsymbol{x_1}, \boldsymbol{x_2}, \boldsymbol{x_3}), i = 1, 2 \tag{9.4}$$

The values $f_i(\boldsymbol{x_1}, \boldsymbol{x_2}, \boldsymbol{x_3})$ will be the reattachment length or the P' integral value in Problem 1 and Problem 2, or both the reattachment length and the P' integral value for the Problem 3.

The values $f_{pi}(\boldsymbol{x_1}, \boldsymbol{x_2}, \boldsymbol{x_3})$ and $f_{ei}(\boldsymbol{x_1}, \boldsymbol{x_2}, \boldsymbol{x_3})$ are the prescribed value and the evaluated value for the objective functions respectively for each of the 3 problems defined, which will define the Reattachment length and/or P' integral value).

Subject to the definition of the vector search space three design parameters $(\boldsymbol{x_1}, \boldsymbol{x_2}, \boldsymbol{x_3})$:

– $\boldsymbol{x_1}$: Voltage (V); $\mathrm{V} \in \mathbb{N},\ 14 \leq \mathrm{V} \leq 20$
– $\boldsymbol{x_2}$: Burst Frequency (f_{bm}, in kHz); $f_{bm} \in \mathbb{N},\ 10 \leq f_{bm} \leq 200$
– $\boldsymbol{x_3}$: Duty Cycle (DC, in %); $\mathrm{DC} \in \mathbb{N},\ 5 \leq \mathrm{DC} \leq 95$.

These inverse problems are solved as traditional reconstruction problems with the main characteristic that the final solution is known from a direct numerical simulation for given values of the triple $\boldsymbol{x_1}, \boldsymbol{x_2}, \boldsymbol{x_3}$. Thus, the recovery of the prescribed solution validates the operability of the optimization procedure.

Figures 9.7, 9.8 and 9.9 show the convergence history of the main objective functions for each of the three test case problems (1), (2) and (3). All three figures are plotting the convergence of the best individual along the iteration process of the optimizer. Figure 9.7 shows the deviation to zero of the difference between the real reattachment length and the evaluated one, Fig. 9.8 between the real P' and the evaluated one respectively. Figure 9.9 shows the main objective function of the multi-objective problem solved. It shows the convergence to zero of the difference

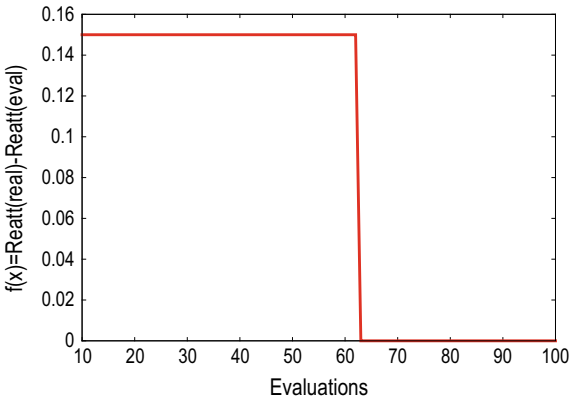

Fig. 9.7 Convergence history for problem: matching the reattachment length

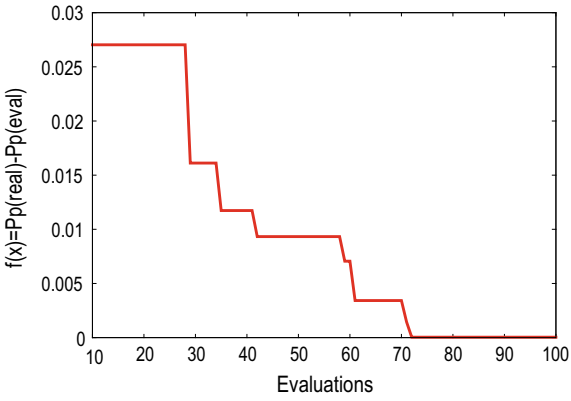

Fig. 9.8 Convergence history for problem 2, recover of P'

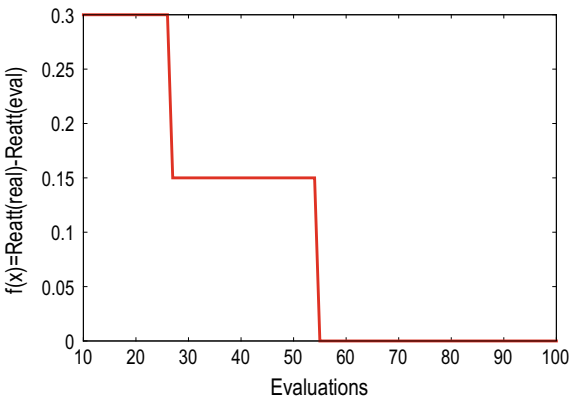

Fig. 9.9 Convergence history of the reattachment length for the problem 3; Reconstruction of the reattachment length and P'

between the real reattachment length and the evaluated one. In all three cases, the deviation value of the inverse problems is 0, and the prescribed design variables values of the direct simulation are fully matched by the converged solutions.

The GAs optimizer coupled with the Experimental Plasma active device captures the solution of Problem 1. The solution of the problem is capturing the evaluated value which compared to the prescribed value leads to a deviation of the objective function equal to zero. Regarding the design variables, the three parameters that recover the optimal individual:

– Voltage was 20 V and the obtained values is 20 V,
– Burst Frequency was 130 kHz, and the obtained one is 130 kHz,
– And finally the Duty Cycle was 60%, the same for the obtained one.

The solution of the Problem 2 also shows a good agreement with the prescribed values. The difference is 0.00004 in this case. Regarding the design variables, the three parameters that recover the optimal individual:

– Voltage was 20 V as well as the converged value,
– Burst Frequency was 70 kHz while the converged one is 72 kHz,
– And finally the Duty Cycle was defined between 60% and 70%, while the converged one is 52%.

The solution of Problem 3 also shows the best possible agreement with the prescribed values. The computed deviation with both the objective functions is zero. Regarding the design variables, the three parameters match quite well the prescribed variables:

– Voltage was 20 V and the converged values are 19 V,
– Burst Frequency was 130 kHz, and a similar converged value can be noticed,
– And the Duty Cycle was 60%, while the converged one is 55%.

The experimental-numerical methodology has been validated with a good agreement with the prescribed values defined by direct simulation. It should take into consideration that the precision of the wind tunnel is not able to distinguish among close values and the solution to obtain a prescribed value is not unique. It means that several combinations of V, f_{bm} and DC can lead to the same reattachment or P' integral values. It also should be taken into consideration the limit of operability of the Plasma Wind Tunnel. To avoid equipment damages, it has been requested to limit the time operability of the Plasma Wind tunnel to one hour during the optimization procedure. Considering that each wind tunnel shot evaluation necessitates about 5–10 s, only one hundred evaluations of the GAs population is allowed. The optimizer restarts the search to a pre-defined point to cope with the time limitation. As shown by convergence results obtained with best individuals of the GAs population, it was not necessary to use the restart option thanks to a fast convergence of all the three reconstruction problems.

9.4.2 *Optimization Problems with Plasma Wind Tunnel Analysis*

An optimization test case problem has been set up to complete the analysis of the efficiency of the experimentally coupled optimization procedure. It selects the P' integral value as the objective function. From the physical point of view of the plasma device set up analysis, the P' value is a sensitive parameter to control the flow, as described in Sect. 9.2.

The optimization problem is now defined as:

Maximize

$$f_o(\vec{x}) = \max\left[P'(\vec{x})\right], \tag{9.5}$$

where $\vec{x}$ is the vector containing the three design parameters of the plasma wind tunnel device.

The optimization problem, defined by Eq. (9.5), is defined as a single-objective maximization problem, with the following definition of the lower-upper bounds search space of the three design parameters:

- Voltage (V); $V \in \mathbb{N},\ 14 \leq V \leq 20$
- Burst Frequency (f_{bm}, in kHz); fbm $\in \mathbb{N},\ 10 \leq f_{bm} \leq 200$
- Duty Cycle (DC, in %); $DC \in \mathbb{N},\ 5 \leq DC \leq 95$.

The optimized results using the Experimental- GAs optimizer are shown in Fig. 9.10, where the convergence of the P' value to the optimum is shown. As it happened in the previous reconstruction problems, a time limitation had to be set up for the safe operability of the Plasma Wind Tunnel. Once again, a fast convergence of the P' values to the optimum made unnecessary to use the restart option. The plot shows the comparison between the maximized value and the baseline design. The optimized value of P' is 2.247, while the baseline design defines a P' equal to 2.211. It means that the improvement is of 1.6%. The converged best individual of

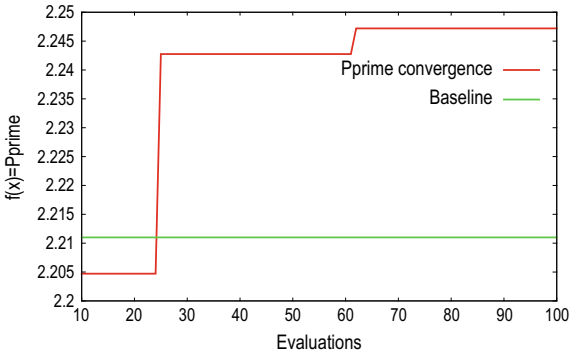

Fig. 9.10 Convergence history of the P' in the GAs maximization with Plasma Wind Tunnel analysis

the population is defined by a Voltage equal to 20 V, a burst frequency of 81 Hz, and a duty cycle of 63%.

9.5 Conclusion and Future

The Plasma Wind tunnel analysis coupled to an evolutionary optimization procedure is an innovative research. It uses the wind tunnel as an analogic solver, mastering the difficulties of coupling Plasma experimental facilities with an evolutionary optimizer. This approach proposes an efficient alternative to the expensive CFD analysis cost. In the selected BFS test case, the coupling between the Plasma Wind tunnel and the optimizer enables a very fast and quasi-real-time estimator of active candidate flow conditions only constrained by limitations in the Plasma wind tunnel equipment which were not necessary in these simple inverse and optimization problems.

The obtained results are relevant to demonstrate the reliability and fast convergence of the approach dealing with inverse and optimization problems. The definition of a multi-objective inverse optimization does not present a major problem and it also converges quickly and accurately.

From the results achieved further research activities on this dual experimental-Numerical approach are planned namely the management of the precision of wind tunnel parameters and the coding of design variables, the choice of other design variables and/or objectives functions.

In this context other more complex multi objective optimization test cases are envisaged with advanced hybridized EAs and Game strategies.

Acknowledgements This research has been partially funded by the European Commission (EC), though the Framework Programme 7 (FP7) and the Ministry of Industry and Information Technology of the People Republic of China (MIIT), Project # 266326 entitled: "Manipulation of Reynolds Stress for Separation Control and Drag Reduction" (MARS).

References

1. Schubauer GB, Skramstad HK (1947) Laminar boundary-layer oscillations and transition on flat plate. United States Bureau of Standards. J Res, 69–78
2. MARS project, FP7 project number 266326. www.cimne.com/mars
3. Benard N, Moreau E (2012) EHD force and electric wind produced by plasma actuators used for airflow control. AIAA paper 3136
4. Eaton JK, Johnston JP (1981) A review of research on subsonic turbulent flow reattachment. AIAA J 19
5. Lee DS, Gonzalez LF, Periaux J, Bugeda G (2011) Double shock control bump design optimisation using hybridised evolutionary algorithms. Special Issue J Aerosp Eng 225(10):1175–1192. https://doi.org/10.1177/0954410011406210

6. Lee DS, Morillo C, Bugeda G, Oller S, Onate E (2011) Multilayered composite structure design optimisation using distributed/parallel multi-objective evolutionary algorithms. J Compos Struct. https://doi.org/10.1016/j.compstruct.2011.10.009
7. Lee DS, Periaux J, Onate E, Gonzalez LF (2011) Advanced computational intelligence system for inverse aeronautical design optimisation. In: International Conference on advanced software engineering (ICASE-11), Proceedings of the 9th IEEE international symposium on parallel and distributed processing with applications workshops, ISPAW 2011—ICASE 2011, SGH 2011, GSDP 2011, Busan, Korea, 26–28 May, 2011, pp 299–304. ISBN 978-1-4577-0524-3. https://doi.org/10.1109/ispaw.2011.46
8. Lee DS, Periaux J, Gonzalez LF. UAS mission path planning system (MPPS) using hybrid-game coupled to multi-objective optimiser. J Dyn Syst Meas Control. DS-09-1135
9. Deb K, Agrawal S, Pratap A, Meyarivan T (2002) A fast and elitist multi-objective genetic algorithm: NSGA-II. IEEE Trans Evol Comput 6(2):182–197
10. Lee DS, Gonzalez LF, Periaux J, Srinivas K. Hybrid-game strategies coupled to evolutionary algorithms for robust multidisciplinary design optimization in aerospace engineering. IEEE Trans Evol Comput. TEVC-00213-2009
11. Periaux J, Lee DS, Gonzalez LF, Srinivas K (2009) Fast reconstruction of aerodynamic shapes using evolutionary algorithms and virtual nash strategies in a CFD design environment. Special Issue J Comput Appl Math 232(1):61–71. ISSN 0377-0427